International Journal of Biological Macromolecules 226 (2023) 780–792

Contents lists available at ScienceDirect

International Journal of Biological Macromolecules

journal homepage: www.elsevier.com/locate/ijbiomac

Ginkgolic acids inhibit SARS-CoV-2 and its variants by blocking the spike protein/ACE2 interplay

Yusen Xiang [a,1], Guanglei Zhai [b,1], Yaozong Li [c,d], Mengge Wang [a], Xixiang Chen [a,e], Ruyu Wang [a], Hang Xie [f], Weidong Zhang [a,g], Guangbo Ge [a], Qian Zhang [h], Yechun Xu [i], Amedeo Caflisch [c], Jianrong Xu [e,j,*], Hongzhuan Chen [a,*], Lili Chen [a,*]

[a] Shanghai Frontiers Science Center of TCM Chemical Biology, Institute of Interdisciplinary Integrative Medicine Research, Shanghai University of Traditional Chinese Medicine, Shanghai 201203, China
[b] Shanghai HighsLab Therapeutics. Inc., Shanghai 201203, China
[c] Department of Biochemistry, University of Zurich, Winterthurerstrasse 190, CH-8057 Zurich, Switzerland
[d] Department of Chemistry, Umeå University, SE-901 87 Umeå, Sweden
[e] Academy of Integrative Medicine, Shanghai University of Traditional Chinese Medicine, 1200 Cailun Road, Shanghai 201203, China
[f] School of Chinese Materia Medica, Nanjing University of Chinese Medicine, Nanjing 210023, China
[g] Shanghai Institute of Infectious Diseases and Biosafety, Institute of Interdisciplinary Integrative Medicine Research, Shanghai University of Traditional Chinese Medicine, Shanghai 201203, China
[h] Department of Medicinal Chemistry, School of Pharmacy, Fudan University, Shanghai 201203, China
[i] CAS Key Laboratory of Receptor Research, State Key Laboratory of Drug Research, Shanghai Institute of Materia Medica, Chinese Academy of Sciences, Shanghai 201203, China
[j] Shanghai Universities Collaborative Innovation Center for Translational Medicine, Shanghai Jiao Tong University School of Medicine, 280 South Chongqing Road, Shanghai 200025, China

ARTICLE INFO

Keywords:
SARS-CoV-2
S-RBD
Ginkgolic acid

ABSTRACT

Targeting the interaction between the spike protein receptor binding domain (S-RBD) of severe acute respiratory syndrome coronavirus 2 (SARS-CoV-2) and angiotensin-converting enzyme 2 (ACE2) is a potential therapeutic strategy for treating coronavirus disease 2019 (COVID-19). However, we still lack small-molecule drug candidates for this target due to the missing knowledge in the hot spots for the protein-protein interaction. Here, we used NanoBiT technology to identify three Ginkgolic acids from an in-house traditional Chinese medicine (TCM) library, and they interfere with the S-RBD/ACE2 interplay. Our pseudovirus assay showed that one of the compounds, Ginkgolic acid C17:1 (GA171), significantly inhibits the entry of original SARS-CoV-2 and its variants into the ACE2-overexpressed HEK293T cells. We investigated and proposed the binding sites of GA171 on S-RBD by combining molecular docking and molecular dynamics simulations. Site-directed mutagenesis and surface plasmon resonance revealed that GA171 specifically binds to the pocket near R403 and Y505, critical residues of S-RBD for S-RBD interacting with ACE2. Thus, we provide structural insights into developing new small-molecule inhibitors and vaccines against the proposed S-RBD binding site.

1. Introduction

The coronavirus disease 2019 (COVID-19) is caused by a novel coronavirus known as severe acute respiratory syndrome coronavirus 2 (SARS-CoV-2) and is spreading rapidly around the world. To date, >600 million confirmed cases of COVID-19, including >6 million deaths, have been reported to the World Health Organization (WHO) (https://covid19.who.int/table). Most patients present with multiorgan symptoms such as shortness of breath, palpitations, joint pain, and headache. In some discharged patients, the dysfunctions and complications may persist for at least six months [1]. Therefore, there is an urgent need to develop new drugs for specific and effective treatment beyond preventive vaccination.

SARS-CoV-2, an enveloped single-stranded RNA β-coronavirus,

* Corresponding authors.
E-mail addresses: janker.xu@gmail.com (J. Xu), yaoli@shsmu.edu.cn (H. Chen), llchen@shutcm.edu.cn (L. Chen).
[1] These authors have contributed equally to this work.

https://doi.org/10.1016/j.ijbiomac.2022.12.057
Received 27 September 2022; Received in revised form 3 December 2022; Accepted 6 December 2022
Available online 12 December 2022

mediates receptor binding and membrane fusion through its surface spike (S) protein [2]. Coronavirus S protein has a transmembrane structure and forms a trimer in its functional state. Proteases can cleave the protein's ectodomain into S1 and S2 subunits [2]. The receptor binding domain (RBD) in S1 subunit can bind to the host cell receptor and cause the conformational change of the S2 subunit, thereby mediating the fusion of the viral and cellular membrane [3]. Many studies have shown that SARS-CoV-2 enters host cells by targeting angiotensin-converting enzyme 2 (ACE2), a type I membrane protein widely expressed in humans, with a higher affinity than that for SARS-CoV binding to ACE2 [4–7]. Therefore, the search for antiviral candidates that target S-RBD/ACE2 interactions has become an obvious priority.

Traditional Chinese medicine (TCM) has shown great potential in preventing and treating COVID-19 as more and more active antiviral TCM ingredients are emerging [8–11]. Lyu et al. summarized and discussed the clinical effects and potential mechanisms of TCM at different disease stages for the treatment of COVID-19, emphasizing the scientific value of TCM in combating COVID-19 [12]. Ginkgolic acid, the main component of *Ginkgo biloba*, has a variety of biological activities, such as antitumor [13], anti-inflammatory [14], antibacterial [15], and broad-spectrum antiviral effects [16–18]. A recent study found that Ginkgolic acid C15:1 (GA151) inhibited several enzymes that play crucial roles in viral polyprotein processing, e.g., 3-chymotrypsin-like protease ($3CL^{pro}$) and papain-like protease (PL^{pro}) [19]. The inhibition affects the SARS-CoV-2 infection and replication [19]. In addition, the inhibitory effect of GA151 on HIV protease protects human peripheral blood mononuclear cells from HIV infection [20]. Moreover, GA151 exhibited a broad-spectrum inhibitory effect on the viral fusion process of several enveloped viruses, such as Herpes Simplex Virus 1 (HSV-1), Human Cytomegalovirus (HCMV), and Zika Virus (ZIKV) [21]. Furthermore, GA151 can inhibit both the production of human coronavirus and the synthesis of viral N protein, which is conserved among the α, β, and γ genera of coronaviruses [18]. Therefore, further study on the antiviral mechanism of Ginkgolic acid is of great significance in exploring effective compounds against SARS-CoV-2.

Computational methods play essential roles in understanding the pathogenesis of COVID-19 and discovering drug candidates against it. For example, molecular dynamics (MD) and free energy simulations were implemented to explore critical residues for the identification between SARS-CoV-2 S-RBD and the host ACE2 [22,23]. Combined with X-ray crystallography, researchers used molecular simulations to understand how variants escape the host immune system, i.e., the omicron variant [24,25]. Furthermore, during the COVID-19 pandemic, several research groups used in silico methods to propose small-molecules to treat the disease against multiple drug targets, i.e., the nonstructural proteins [26–28], $3CL^{pro}$ [29–32], and RNA-dependent RNA polymerase (RdRp) [33,34]. Using small-molecules to target S-RBD is promising among potential therapeutic targets as it could block the ACE2/S-RBD interaction. S-RBD is unique for the coronavirus; thus, targeting it could reduce the possibility of suffering side effects. Recent studies have made efforts in this direction [35,36].

Here, we screened our in-house TCM library by NanoBiT technique and discovered three Ginkgolic acid compounds that show the activity of blocking SARS-CoV-2 S-RBD/ACE2 interaction. Our experiments showed that one of the compounds Ginkgolic acid C17:1 (GA171) exhibited potent inhibitory activity against SARS-CoV-2-S pseudovirus with low cytotoxicity. We confirmed the binding sites of the compound by combining molecular simulations and multiple biological and biophysical experiments. One binding site locates in a particular place of S-RBD that blocks its interaction with ACE2. This study shows an example for the first time that a drug-like small-molecule can bind S-RBD and potentially block the viral invasion to the human cell via the binding to the protein ACE2.

2. Materials and methods

2.1. Cell culture and cell viability assays

HEK293 and HEK293T cell lines were obtained from ATCC (Manassas, VA, USA). Normal human bronchial epithelial BEAS-2B cells were purchased from EK-Bioscience (Shanghai, China). African green monkey kidney epithelial Vero-E6 cells and HEK293F cells were obtained from the Cell Bank of the Type Culture Collection of the Chinese Academy of Sciences (Shanghai, China). Mouse aorta smooth muscle cells (MASMCs) were a kind gift from Professor Jiange Zhang from Shanghai University of Traditional Chinese Medicine, China. All adherent cells were routinely maintained in Dulbecco's modified Eagle's medium (DMEM) supplemented with 10 % fetal bovine serum (FBS), 100 U/mL penicillin, and 100 μg/mL streptomycin in a humidified atmosphere containing 5 % CO_2 at 37 °C. HEK293F cells were grown in OPM-293 CD05 medium (OPM Biosciences, Shanghai, China), cultured at 37 °C with 8 % CO_2 and 125 rpm in an orbital shaking incubator.

For cell toxicity assays, the cytotoxicity of the test compound to BEAS-2B, Vero-E6, and MASMCs was determined by Cell Counting Kit-8 (CCK-8, Meilunbio, Dalian, China). In brief, 50 μL cell suspensions were added to each well of 96-well plates. After 12 h of incubation, cells were pretreated with 10 μL 10× compounds at 37 °C for 1 h, and 40 μL medium was added to each well. After 24 h of incubation, the culture medium was refreshed, and the cells were incubated for another 24 h. Then the medium was replaced with CCK-8 solution according to the manufacturer's instructions. The OD value was measured at a wavelength of 450 nm (BioTek, Winooski, USA).

2.2. Pseudovirus production

The recombinant plasmid expressing SARS-CoV-2 spike protein (pcDNA3.1-SARS-CoV-2-S) and plasmids including pAX2, pHB-Rluc, pcDNA3.1-ACE2 were obtained from Precedo (Anhui, China). The codon-optimized expression plasmid encoding full-length spike protein of Omicron SARS-CoV-2 was purchased from GenScript (Nanjing, China) and the plasmids expressing spike protein of Delta (Cat. No. #172320), and Gamma (Cat. No. #170450) of SARS-CoV-2 were from Addgene (Watertown, MA, USA). The SARS-CoV-2 pseudovirus was generated as previously described [37]. Briefly, HEK293T cells were co-transfected with three plasmids using the LipoFiter 3.0 transfection reagent (Hanbio, Shanghai, China) according to the manufacturer's instructions. After 6 h, the culture medium was replaced with fresh DMEM. After 48 h, the supernatant containing pseudovirus was collected by centrifuge (3000 *g*, 10 min) and filtered with 0.45 μm membrane (Jet Bio-Filtration, Guangzhou, China). Use the pseudovirus immediately or store at −80 °C in 1 mL aliquots until use.

2.3. Pseudovirus neutralization assays

HEK293T cells were seeded in 96-well plates after transient transfection with pcDNA3.1-ACE2 plasmid by the LipoFilter 3.0 transfection reagent. For the neutralization assay, hACE2/HEK293T cells were pre-incubated with the test compounds at 37 °C for 1 h, then SARS-CoV-2 pseudovirus and Polybrene (6 μg/mL) (Absin, Shanghai, China) were added to each well and incubated for 24 h. Then, the culture medium was refreshed, and 30 μL Renilla luciferase Reagent (Promega, Madison, WI, USA) was added into each well after 48 h postinfection. The contents were mixed on an orbital shaker for 2 min to induce cell lysis, and the relative luciferase activity was detected using a Multilabel Reader (SpectraMax Paradigm, Molecular Devices, CA, USA). The Relative Luminescence (%) was calculated according to the procedures recommended by the manufacturer. The half-maximal inhibitory concentration (IC_{50}) values were calculated by non-linear regression analysis using GraphPad Prism 8.0 (San Diego, CA, USA).

2.4. NanoBiT assay

NanoBiT assays were performed as previously described [37]. Briefly, HEK293 cells were co-transfected using FuGENE HD transfection reagent (Promega, Madison, WI, USA) with SARS-CoV-2 S-RBD-LgBiT and SmBiT-ACE2 plasmids according to the manufacturer's instructions. Cells were incubated for 6 h at 37 °C with a transfection medium. Cells were then reseeded into a 96-well white plate with fresh medium for 16 h. Subsequently, the corresponding concentrations of compounds were incubated with the cells at 37 °C for 3 h. Finally, Nano-Glo Live Cell Assay reagent (Promega, Madison, WI, USA) was added to the cells, and luminescence was determined using the Envision plate reader (Perkin Elmer, Waltham, MA, USA). To exclude the interference of the compounds to the NanoBiT system per se, the cytotoxicity of the compounds was measured by CellTiter-Glo (CTG) Luminescent Cell Viability Assay (Promega, Madison, WI, USA), and the inhibitory effects of the compounds on NanoLuc (HEK293/NanoLuc stable cells) were also determined. The activities of the compounds were evaluated by NanoBiT inh% (SARS-CoV-2 S-RBD/ACE2 interaction), NanoLuc inh% (NanoLuc luciferase), and Cytotox inh% (cell proliferation).

2.5. Protein expression and purification

The DNA fragment encoding S-RBD (residues 319–541) was subcloned into the mammalian expression vector pTT5 with a C-terminal 6 × His tag. The high-quality plasmids were transfected into HEK293F cells by PEI (Polysciences, Warrington, PA, USA). After five days of culture, the cell culture supernatant was harvested and purified by Ni-NTA. Purified proteins were analyzed by SDS-PAGE to ensure purity and appropriate molecular weights.

2.6. Binding site prediction of GA171 to S-RBD

The SARS-CoV-2 S-RBD was selected as the binding target. The crystal structure 6M0J was chosen for the model building [38]. Before predicting how GA171 binds to the protein, all crystal water molecules were removed, and glycosylated residue Asn343 was turned to its unmodified form. To determine the appropriate states of the S-RBD residues, we analyzed the interaction between S-RBD and ACE2 by Maestro [39]. The states of S-RBD's interfacial residues that interact with ACE2 were determined by considering the protein-protein interactions. After checking the hydrogen binding networks of the complex structure, titratable residues were turned to their correct states, which was assisted by the pKa prediction from PROPKA3 [40]. The orientation of polar residues was also determined by the interaction analysis and flipping along their original planes, for example, histidine, asparagine, and glutamine. Finally, chain E of 6M0J, i.e., the S1 sub-domain of S-RBD ranging from T333 to G526, was extracted from the complex crystal structure of viral protein's S-RBD bound to ACE2.

The chemical structure of GA171 was drawn by MarvinSketch [41], and its most populated protonation state in the aqueous solution was determined according to its predicted micro pKa values by the "Cxcalc" module of ChemAxon [41]. The 3D model of the ligand was generated by the "Molconvert" module of ChemAxon [41]. The hydroxyl and carboxyl groups on the benzene ring were protonated and deprotonated, respectively.

The initial poses were sampled by the docking software Smina [42], a fork of Autodock Vina with improved flexibility [43]. The docking site was defined by a 100 × 100 × 100Å cubic grid box and centered on the S-RBD coordinates (x-axis: −32.38; y-axis: 25.84; y-axis: 21.45). This relatively large size of the grid box ensures embodying the entire structure during the docking simulations. The parameter "exhaustiveness" was set to 200 to enhance the configurational sampling of binding poses. The rest of the parameters were left as the default. Finally, all 200 docking poses were output for further analysis.

The 200 docking poses mainly emerged on five different sites of the protein surface. For each potential binding site suggested by the docking simulations, we only considered the first two best-ranked poses for further MD simulations. In total, ten protein-ligand complex systems were constructed. Each of the S-RBD-GA171 modeled complex structures was solvated in an 88 Å rhombic dodecahedron TIP3P water box [44], which ensured a 12 Å buffer distance between protein atoms and water box boundary. 0.15 M of sodium chloride was added to the water box to neutralize the protein-ligand system and mimic the physiological condition. The CHARMM36m force field was used to describe the S-RBD protein, and GA171was parametrized by the CGenFF force field [45,46].

Each complex system was initially minimized to 10,000 steps by mixing the conjugate gradient and adopted basis Newton Raphson algorithms under a series of restraints and constraints to remove its unreasonable contacts and geometry. The minimized structure was heated to 300 K and equilibrated in an NVT condition (constant volume and temperature). Finally, the structure was further equilibrated in an NPT condition (constant pressure and temperature). The heating-up and equilibration phases lasted for one ns using the CHARMM program (version 42b1) [47]. Production MD simulations were continued in NPT conditions. The pressure was controlled at 1 atm by the Nosé–Hoover Langevin piston method [48,49]. The temperature was maintained at 300 K using the Nosé–Hoover thermostat [50]. The masses of temperature and pressure pistons were kept at 20 % and 2 % of the system mass, respectively. The integration time step was set to 2 fs by fixing all bonds connecting hydrogen atoms by the SHAKE algorithm [51]. Van der Waals energies were calculated using a switching function with a switching distance from 10 to 12 Å. Electrostatic interactions were evaluated using the particle mesh Ewald summation (PME) method with a 1 Å of grid spacing [52]. Each system was simulated for 5 ns, and three independent runs with the same initial coordinates and random velocities were carried out. Thus, a cumulative sampling of 15 ns trajectories (1500 snapshots saved every 10 ps) was collected from each system. Time-evolved root-mean-square deviation (RMSD) values and average structure were calculated based on the 1500 snapshots of each system.

2.7. Alanine scanning validation

For single-point mutations on S-RBD, including R346A, R403A, T430A, Y505A, and Y505H, the corresponding residues were substituted by Ala or His. All mutant plasmids were constructed using the Mut Express II Fast Mutagenesis Kit V2 (Vazyme, Guangzhou, China) according to the manufacturer's instructions. After all mutant plasmids were sent to Sangon Biotech (Shanghai, China) for nucleic acid sequencing, the proteins were generated using HEK293F expression system and purified as described above.

2.8. Circular dichroism

The circular dichroism (CD) spectra were used to explore the secondary structure of SARS-CoV-2 S-RBD and its mutants on BRIGHT TIME Chirasca (Applied Photophysics, Britain) spectropolarimeter. Proteins in phosphate-buffered saline (PBS) were recorded at 25 °C in a quartz cell of 0.5 mm path length. The concentration of proteins was 0.5 mg/mL, and the spectrum was recorded at wavelengths between 200 and 260 nm. The spectra represent an average of three corrected scans. The analysis of secondary structure content was performed using CDNN software (version 2.1).

2.9. Surface plasmon resonance assay

Biacore T200 instruments (Cytiva) were used to evaluate the binding affinity of the compounds to human ACE2 (10108-H05H, Sino Biological, Beijing, China), SARS-CoV-2 S-RBD and the S-RBD mutants via surface plasmon resonance (SPR), as previously described [37]. Briefly, all the proteins were immobilized on the different channels of the CM5 chip by using an amine-coupling approach at a flow rate of 10 μL/min in

10 mM sodium acetate buffer (pH 4.0), respectively. The sensor surface was activated with a 7 min injection of the mixture of 50 mM N-hydroxysuccinimide (NHS) and 200 mM 1-ethyl-3-(3-dimethylaminopropyl) carbodiimide (EDC). Then 10 μg/mL of human ACE2 and 50 μg/mL of S-RBD or mutants were injected for 420 s, and the surface was blocked with 1 M ethanolamine, pH 8.5. Series concentrations of the compounds were injected into the flow system and analyzed for 90 s, and the dissociation was 120 s. As for the binding affinity of S-RBD mutants to human ACE2, the association time was set to 120 s, while the dissociation time was set to 300 s. All binding analysis was performed in PBS with 0.05 % (*v*/v) Tween-20 and 1 % DMSO, pH 7.4, at 25 °C. Prior to analysis, double reference subtractions and solvent corrections were made to eliminate bulk refractive index changes, injection noise, and data drift. The binding affinity was determined by fitting a Langmuir 1:1 binding model within the Biacore Evaluation software (Cytiva).

2.10. Statistical analysis

Data are presented as mean ± standard deviation (SD). Statistical differences were analyzed and determined based on *P*-values (* $p < 0.05$, ** $p < 0.01$, and *** $p < 0.001$).

3. Results

3.1. Ginkgolic acids exhibit inhibitory activity against SARS-CoV-2-S pseudovirus

To screen effective inhibitors that block SARS-CoV-2 S-RBD/ACE2 interaction, we used the NanoBiT-based high-throughput system to screen 115 compounds at the concentration of 50 μM and Niclosamide (Nic) was used as a positive compound (Fig. S1) [53,54]. After the selection, six candidate compounds were identified, which showed an

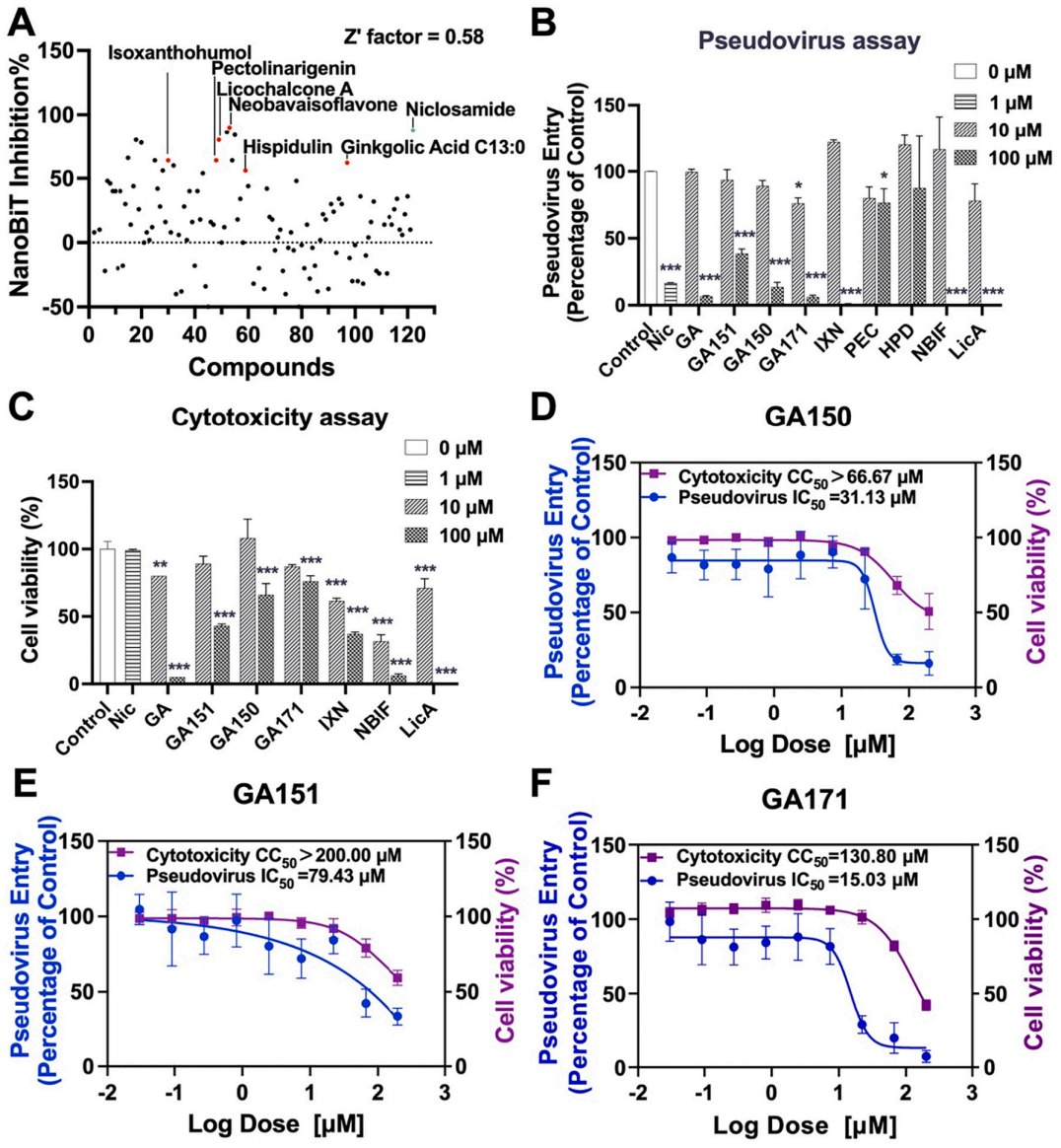

Fig. 1. Screening of the compounds and evaluation of anti-SARS-CoV-2-S pseudovirus activities and cytotoxicities. (A) Six compounds were screened as potent SARS-CoV-2 S-RBD/ACE2 interaction inhibitors. (B-C) Antiviral activities and cytotoxicities of Ginkgolic acid C13:0 (GA), Ginkgolic acid C15:1 (GA151), Ginkgolic acid C15:0 (GA150), Ginkgolic acid C17:1 (GA171), Isoxanthohumol (IXN), Pectolinarigenin (PEC), Hispidulin (HPD), Neobavaisoflavone (NBIF), Licochalcone A (LicA), and the positive compound Niclosamide (Nic) in preliminary screening. IC_{50} and CC_{50} values of (D) GA150, (E) GA151, and (F) GA171 were determined.

inhibitory effect on S-RBD/ACE2 interaction (Fig. 1A). Among the six compounds, Ginkgolic acid C13:0 (GA) exhibited a strong blocking activity (Inhibition rate = 62 %). We therefore considered another three derivatives of GA, including Ginkgolic acid C15:0 (GA150), GA151, and GA171, for the following pseudovirus neutralization assay. We performed the assay to evaluate the ability of the nine compounds to block SARS-CoV-2-S pseudovirus infection in hACE2/HEK293T cells. The results showed that seven compounds including GA, GA151, GA150, GA171, Isoxanthohumol (IXN), Neobavaisoflavone (NBIF), and Licochalcone A (LicA), exhibited anti-pseudovirus activities at a 100 μM concentration. By contrast, Pectolinarigenin (PEC) and Hispidulin (HPD) had no significant antiviral activities at either 10 or 100 μM (Fig. 1B). We then investigated the cytotoxicities of these seven compounds to hACE2/HEK293T cells to exclude false positive results through CTG assay. The results showed that four compounds had strong cytotoxic effects on hACE2/HEK293T cells except for GA150, GA151, and GA171 (Fig. 1C). We further assessed the inhibitory activities of the three compounds against SARS-CoV-2-S pseudovirus and their cytotoxicities to hACE2/HEK293T cells. As shown in Fig. 1D-F, GA150, GA151, and GA171 exhibited a dose-dependent inhibition of SARS-CoV-2-S pseudovirus, resulting in IC_{50} values of 15.03, 31.13 and 79.43 μM, respectively. The half-maximal cytotoxic concentration (CC_{50}) value of GA151 was over 200 μM, demonstrating its low cytotoxicity to hACE2/HEK293T cells. The CC_{50} values of GA171 and GA150 were 130.80 and over 66.67 μM, respectively. Notably, the selectivity index (SI, defines as $[CC_{50}]/[IC_{50}]$) of GA171 (SI = 8.70) is much higher than that of GA150 (SI > 2.14) and GA151 (SI > 2.52), suggesting that GA171 has more potential than GA150 and GA151.

3.2. Ginkgolic acids interfere with the S-RBD/ACE2 interaction

Based on the results from the pseudovirus assay, we further determined IC_{50} values of the three compounds with serially-diluted concentrations for SARS-CoV-2 S-RBD/ACE2 interaction (NanoBiT inh%), NanoLuc luciferase (NanoLuc inh%) and CC_{50} values for the cytotoxicity (Cytotox inh%) on HEK293 cells (Fig. 2A-C). GA171 exhibited the most potency for inhibiting S-RBD/ACE2 interaction (NanoBiT IC_{50} = 28.17 μM) despite sharing similar cytotoxicity with the other two inhibitors (Fig. 2C). Thus, GA171 deserves further investigation due to its distinguished properties on inhibitory effect on S-RBD/ACE2 interaction, the anti-SARS-CoV-2-S pseudovirus activity, and the maximum SI value.

3.3. Determining the interactions between Ginkgolic acids and SARS-CoV-2 S-RBD or ACE2 by SPR assay

To understand how the compounds block the S-RBD/ACE2 interaction, we utilized SPR assay to detect whether they could directly bind to S-RBD or ACE2. As shown in Fig. 3, GA150, GA151, and GA171 can bind

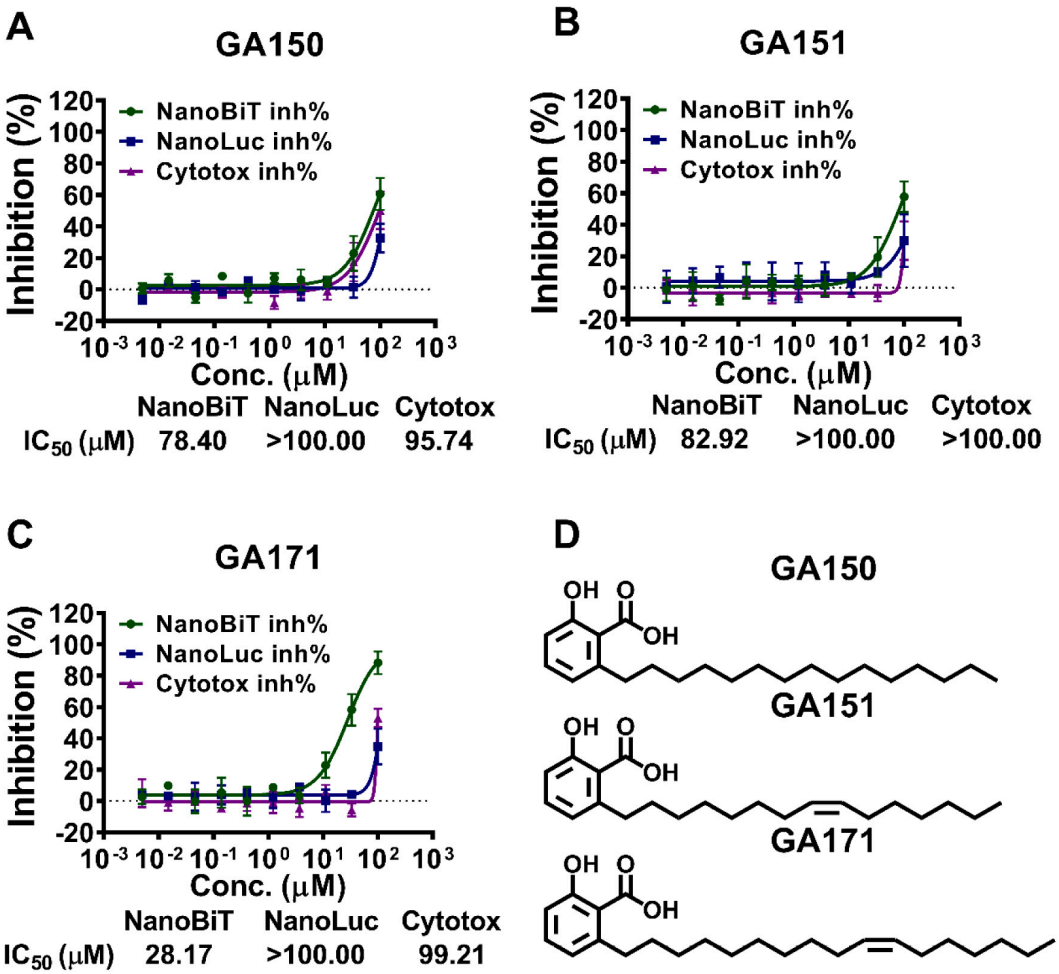

Fig. 2. NanoBiT-based validation of SARS-CoV-2 S-RBD/ACE2 interaction inhibitors. Effect of (A) GA150, (B) GA151, and (C) GA171 on NanoBiT-based SARS-CoV-2 S-RBD/ACE2 interaction. NanoBiT inh%: the inhibition rates against SARS-CoV-2 S-RBD/ACE2 interaction; NanoLuc inh%: the inhibition rates against NanoLuc luciferase; Cytotox inh%: the inhibition rates against the transfected HEK293 cells proliferation. (D) The chemical structure of GA150, GA151, and GA171. $n = 3$.

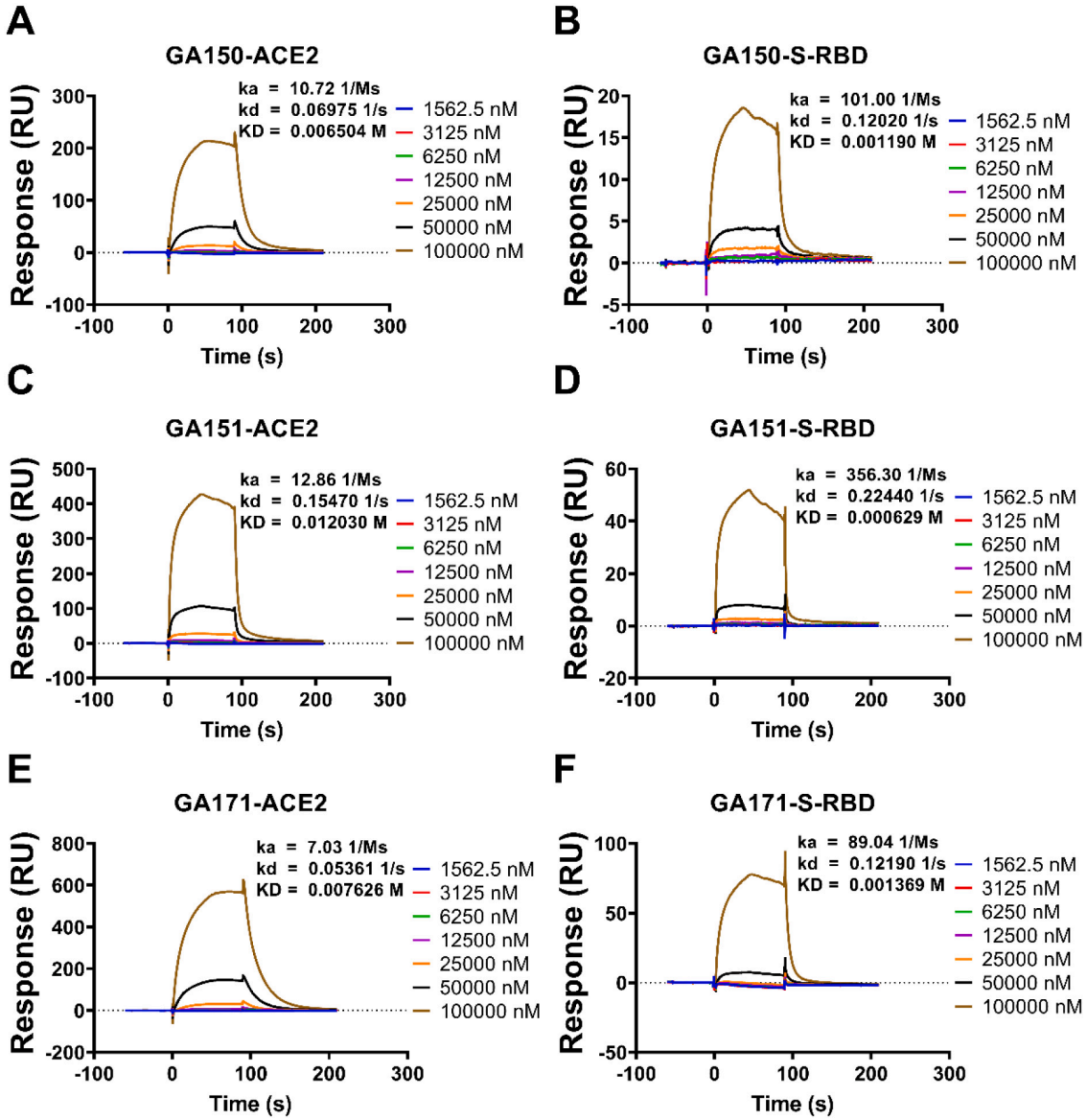

Fig. 3. Compounds bound to SARS-CoV-2 S-RBD or ACE2. Interactions of SARS-CoV-2 S-RBD or ACE2 with the compounds measured by SPR. The SARS-CoV-2 S-RBD or ACE2 was coated on the CM5 sensor chip, and serial dilutions of the compounds (1562.5, 3125, 6250, 12,500, 25,000, 50,000, and 100,000 nM) were used as analytes. Changes in plasmon resonance are shown as response units. Binding curves (colored lines) were obtained by passing different concentrations of GA150 (A), GA151 (C), and GA171 (E) over immobilized ACE2. Binding curves (colored lines) were obtained by passing different concentrations of GA150 (B), GA151 (D), and GA171 (F) over immobilized S-RBD.

to SARS-CoV-2 S-RBD and ACE2. Although the compounds' binding affinities are in the millimolar range, the well-shaped binding curves confirmed their association and dissociation processes. In addition, the compounds exhibited faster kinetics and higher affinities when binding to SARS-CoV-2 S-RBD than human ACE2.

3.4. Mapping binding sites of GA171 to S-RBD

To detect the binding sites of Ginkgolic acids, we preferentially selected S-RBD and the compound GA171 as the target and ligand, respectively. We chose S-RBD as the drug target due to the following two factors. First, its druggability has been validated by widely used vaccines and antibodies. Second, S-RBD is a part of the virus protein; thus, targeting it will reduce the possibility of suffering unexpected side effects as targeting human proteins like ACE2. As S-RBD has multiple potential binding cavities on its protein surface, we decided to conduct an unbiased search for the candidate binding sites of GA171; namely, no prior knowledge was used to locate any plausible binding pockets. This so-called "blind" molecular docking simulation provided five potential binding sites of the compound (Fig. 4A and B) [55]. To validate the stability of these docking poses, we conducted multiple short MD simulations (see the method section for details). We evaluated the stability of these docking poses during MD simulations by checking their RMSD values to the corresponding docked poses (Fig. S2). Smaller average RMSD values and their deviation indicate more stable binding poses. The analysis showed that the ligand poses in sites 1, 3, and 5 (Fig. 4C, D, and E) are relatively stable, indicating their pronounced potential as the actual binding pockets (Fig. S2A). The MD-based RMSD analysis can

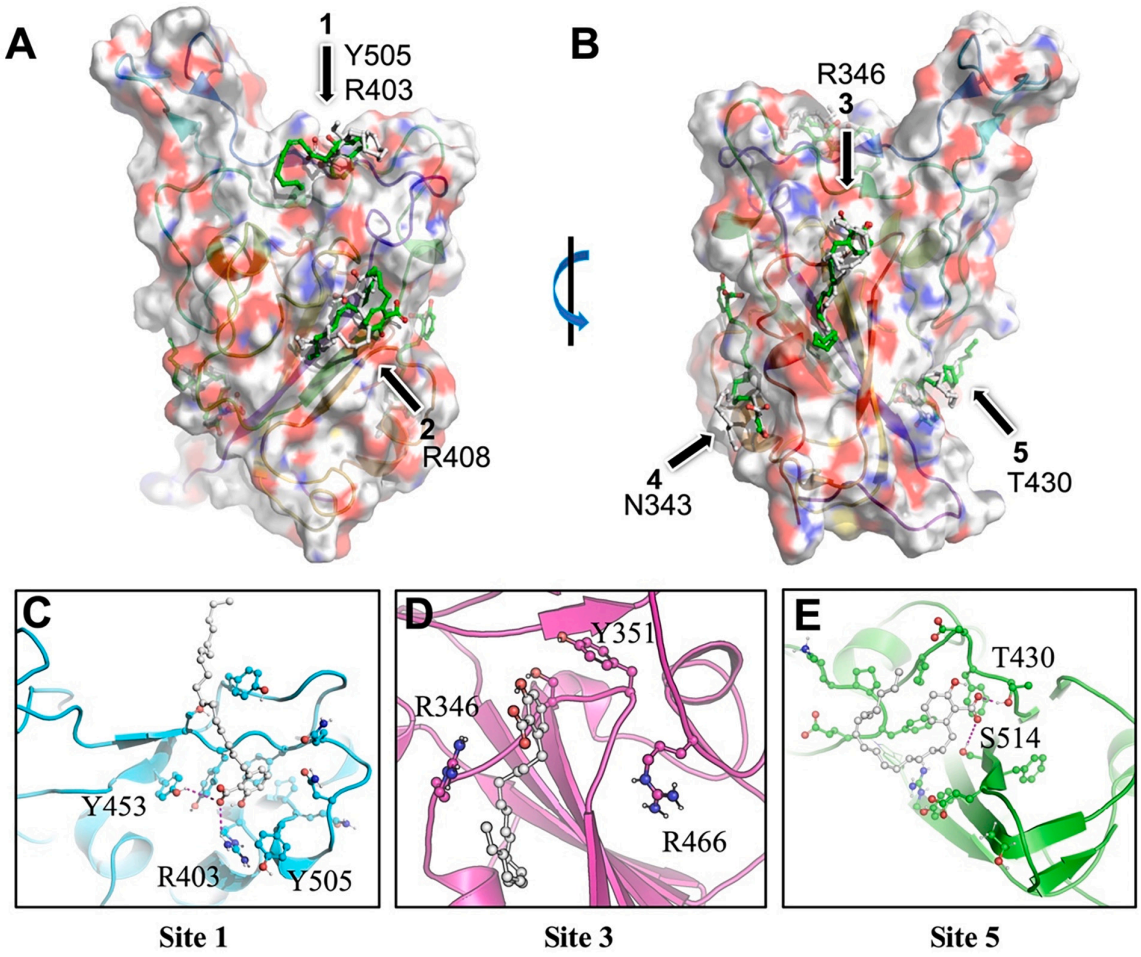

Fig. 4. Potential binding pockets and poses of GA171 to S-RBD. (A-B) Binding poses predicted by molecular docking. For each binding pocket, the best and second best poses ranked by the vina scoring function are colored in light gray and green, respectively. Every pocket is indicated by an arrow with representative residues. The binding pockets and poses were predicted through the "blind" docking mode via Autodock Vina. (C-E) Optimized binding poses by MD simulations after docking. The ligand is shown in a gray ball-and-stick. Three binding sites suggested by MD simulations are shown here, i.e., sites 1, 3, and 5. The structural figures were prepared by PyMOL [57].

efficiently filter out false positives than docking scores [56]. Indeed, the vina docking score cannot distinguish which binding sites GA171 prefers on both wild-type and mutant S-RBD (Fig. S3).

In Fig. S2, we described the rules for proposing residues for further mutagenesis validation. We analyzed the MD-optimized binding modes and identified potential critical residues for the ligand-protein interactions, such as R346, T430, R403, and Y505. We constructed single-point alanine mutations for the four residues to confirm the critical residues for the GA171/S-RBD binding. The four mutant proteins were expressed and purified, and their secondary structures were checked by the Far-UV CD spectra (Fig. 5A and B). The spectra were used to ensure that the binding change of GA171 to mutants is not caused by the proteins' improper folding. Comparative analysis of the spectra between S-RBD's wild-type (WT) and mutants provided similar secondary structure contents. The result indicates that single-point alanine mutations at selected residues do not affect the secondary structures of S-RBD (Fig. 5B and C). We used SPR to measure the binding affinities of the four mutants to GA171. As a result, R403A and Y505A showed approximately 25- and 7-fold reduced binding affinity with GA171, respectively, compared to S-RBD WT (Fig. 5D). T430A underwent an about 6-fold weakened binding. By contrast, R346A did not experience a detectable change. These results indicate that sites 1 and 5 are likely the binding pockets of GA171, but site 3 is not (Fig. 4C-E).

Our model shows that, for site 1, GA171's carboxyl group interacts with R403 by a salt bridge; meanwhile, it also forms a hydrogen bond with Y453 (Fig. 4C). Moreover, Y505 interacts with the salicylic acid aromatic ring by an edge-to-face π-π interaction. In short, the salicylic acid ring is the compound's warhead for the specific recognition by site 1. By contrast, the aliphatic tail of the compound was highly dynamic during the MD simulation and did not show specific interactions with site 1. In site 5 (Fig. 4E), GA171's salicylic acid warhead is recognized explicitly by T430 and S514 via two hydrogen bonds and the aliphatic tail coils in the surface pocket. Because the R403A mutant shows the most significant reduction for the ligand binding, site 1 is probably the primary binding site, and site 5 might be a side pocket.

3.5. GA171 blocks S-RBD/ACE2 interaction by interrupting their interface

The structural analysis shows that some residues of S-RBD may play an essential role in specifically recognizing ACE2, e.g., Y505, Y449, and T500, because they directly contribute to the interaction between the two proteins [38]. For example, S-RBD's Y505 forms two hydrogen bonds with ACE2's E37 and R393 (Fig. 6A). Meanwhile, it also interacts

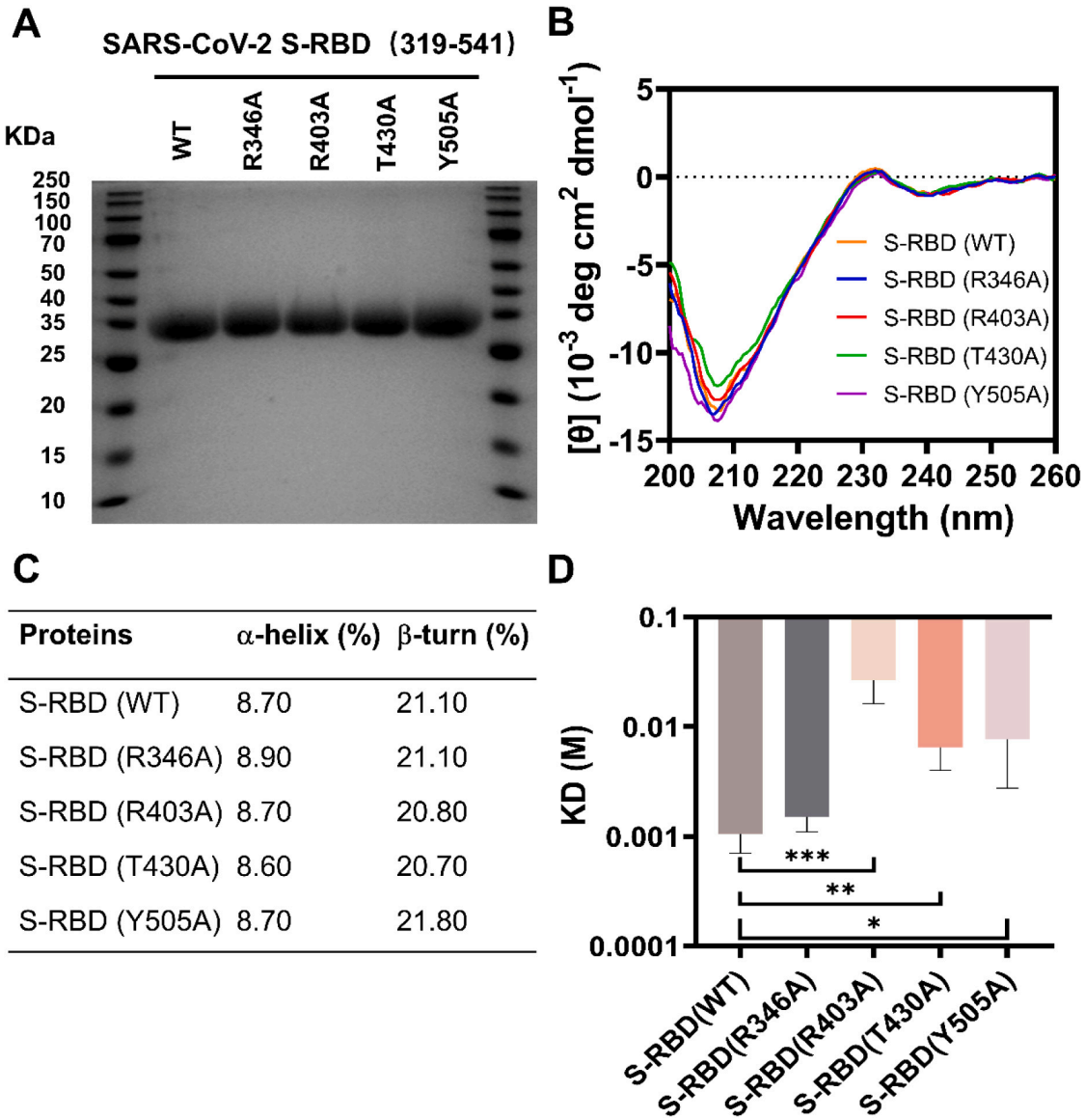

Fig. 5. Binding changes of GA171 to S-RBD mutants. (A) SDS-PAGE of S-RBD WT and mutants (protein purity >95 %). (B) CD spectra of 0.5 mg/mL S-RBD WT and mutants. (C) Secondary structure analysis determined by Far-UV CD spectroscopy. (D) Comparison of the KD values of GA171 among SARS-CoV-2 S-RBD WT and mutants. $^{*}P < 0.05$, $^{**}P < 0.01$, $^{***}P < 0.001$ compared to KD value of GA171 binding to the SARS-CoV-2 S-RBD group.

with the hydrophobic part of ACE2's K353. Interestingly, this site is also predicted to be the GA171's binding site on S-RBD (site 1 in Fig. 4). After superposing the predicted binding pose of the ligand to the heterodimer interface, we find that GA171 interrupts the S-RBD/ACE2 interaction (Fig. 6A). The salicylic acid ring specifically recognizes the S-RBD interfacial site by polar interactions. At the same time, the dynamic aliphatic tail disables the accessibility of ACE2 to S-RBD. This binding mode rationalizes why Ginkgolic acid compounds interfere with the interaction between S-RBD and ACE2 (Fig. 2). Interestingly, the model also suggests the possibility that GA171 blocks the binding of the Omicron S-RBD to ACE2 (Fig. 6B).

The interaction analysis encouraged us to measure the binding affinities of the multiple single-point mutants studied in the last section to ACE2, i.e., R346, T430, R403, and Y505 (Fig. 6C-F, Fig. S4). As a result, the Y505A mutation abolished S-RBD's binding affinity with ACE2, and other alanine mutants weakened the protein's binding strength by ranging about one to three folds. A similar result was also observed in a recent report [58]. The current SARS-CoV-2 variant Omicron has accumulated extensive mutations on S-RBD, evading most existing neutralizing antibodies [59]. Therefore, we mutated Y505 to histidine to mimic the Omicron's S-RBD and determined Y505H's binding affinity with ACE2 by SPR. Consistent with previous studies [60,61], the mutated S-RBD shows an approximately two-fold reduction in binding to ACE2 compared to S-RBD WT (Fig. 6F). Our data confirmed the key residues, including R403 and Y505, for the binding of S-RBD to ACE2 and GA171. More importantly, our results pinpoint the hot spots for the small-molecule targeting by blocking the interplay between S-RBD and ACE2, thus proposing a new strategy to treat COVID-19.

3.6. GA171 inhibits the entry of pseudo-typed SARS-CoV-2 variants into cells

We constructed multiple variant pseudoviruses using the same lentiviral system as SARS-CoV-2-S to determine the capacity of GA171 on

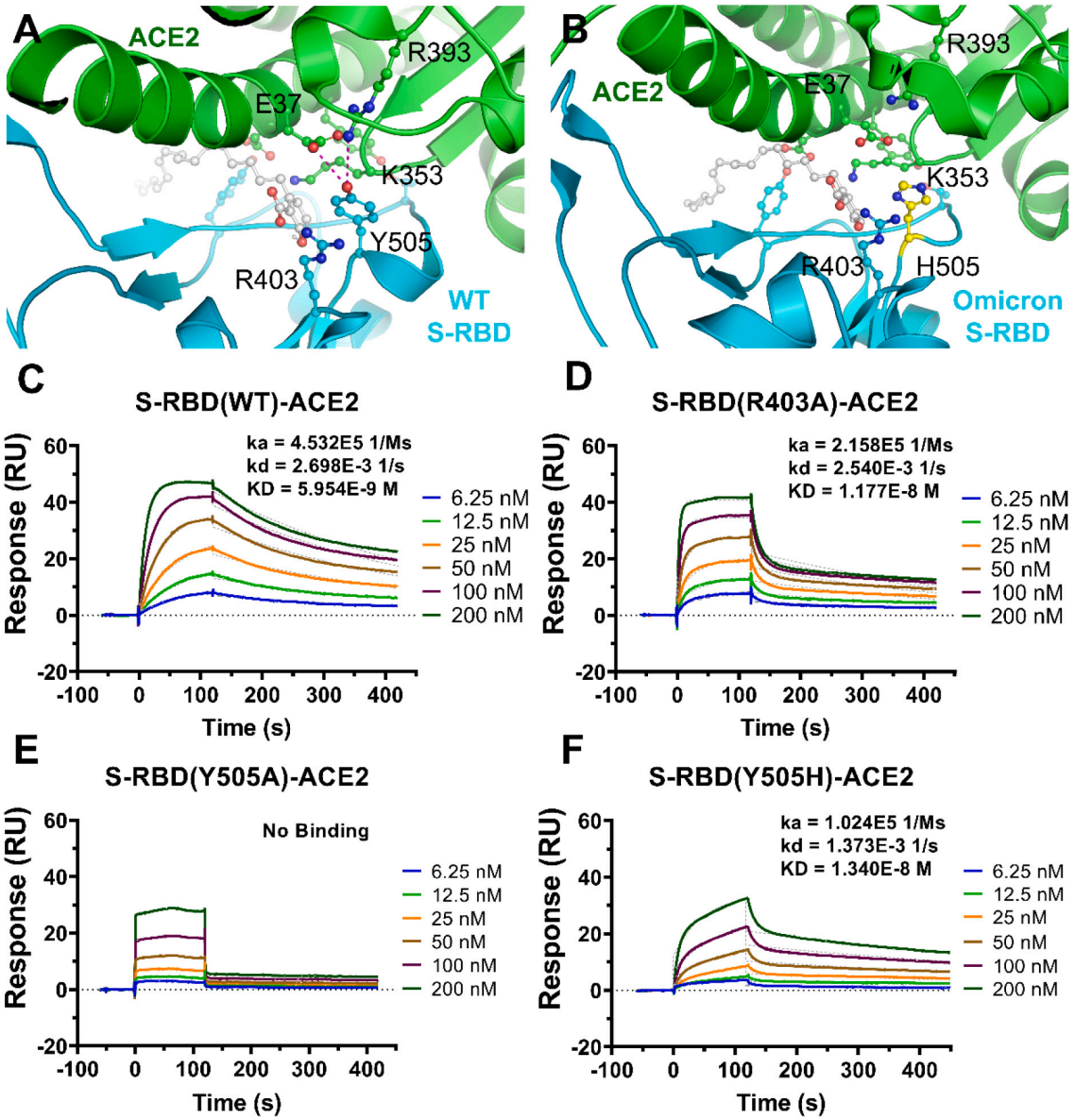

Fig. 6. GA171 interrupts the S-RBD/ACE2 interface. (A-B) Interfacial interactions of ACE2 with S-RBD WT (A) and Y505H mutant (B). The MD-optimized binding pose of GA171 against S-RBD WT (shown in white gray ball-and-stick) is superposed onto the two heterodimer interfaces. The heterodimers of the S-RBD WT and Y505H mutant (Omicron variant S-RBD) are made by crystal structures 6M0J and 7WPB, respectively. For consistency, the sequence numberings of S-RBD of WT and Omicron are kept the same in the figs. (C-F) SPR binding curves (colored lines) were obtained by passing different concentrations of SARS-CoV-2 S-RBD WT and mutants over immobilized ACE2.

antiviral effects against the variants of concern (VOCs), including SARS-CoV-2 Delta, Gamma, and Omicron. We then evaluated the in vitro antiviral efficacy of GA171 against these variants (Fig. 7A). The results indicated that GA171 exhibited similar antiviral activity against these pseudo-typed SARS-CoV-2 strains entering hACE2/HEK293T cells (IC_{50} = 28.25–32.54 μM), including the currently circulating Omicron strains (Fig. 7B and C). Importantly, our data showed that GA171 did not produce significant cytotoxicity to hACE2/HEK293T cells or several typical cell types, including BEAS-2B, Vero-E6, and MASMCs at effective antiviral concentrations (Fig. S5). As described above, GA171 has shown potent antiviral activity against SARS-CoV-2 variants and exhibited no safety concerns in normal cells in vitro, emphasizing its potential as a therapeutic agent for the treatment of COVID-19.

4. Discussion

Ginkgolic acid is a mixture of several 2-hydroxy-6-alkylbenzoic acids, which can be designated as GA, GA150, GA151, and GA171 according to the number of carbon atoms contained in the alkyl chain and the position of the unsaturated bond. Ginkgolic acid is the alkylphenol component of *Ginkgo biloba* extract, which has the potential therapeutic effect, including anti-tumor, anti-inflammatory, and antiviral activities [17]. Previous studies indicated that GA151 has broad-spectrum inhibitory effects on several enveloped viruses by inhibiting viral fusion and protein synthesis [21].

The study by Xiong et al. showed that GA, GA150, GA151, and GA171 have inhibitory effects on SARS-CoV-2 $3CL^{pro}$. At the same time, GA171 and GA150 strongly inhibited SARS-CoV-2 $3CL^{pro}$ in a mixed-

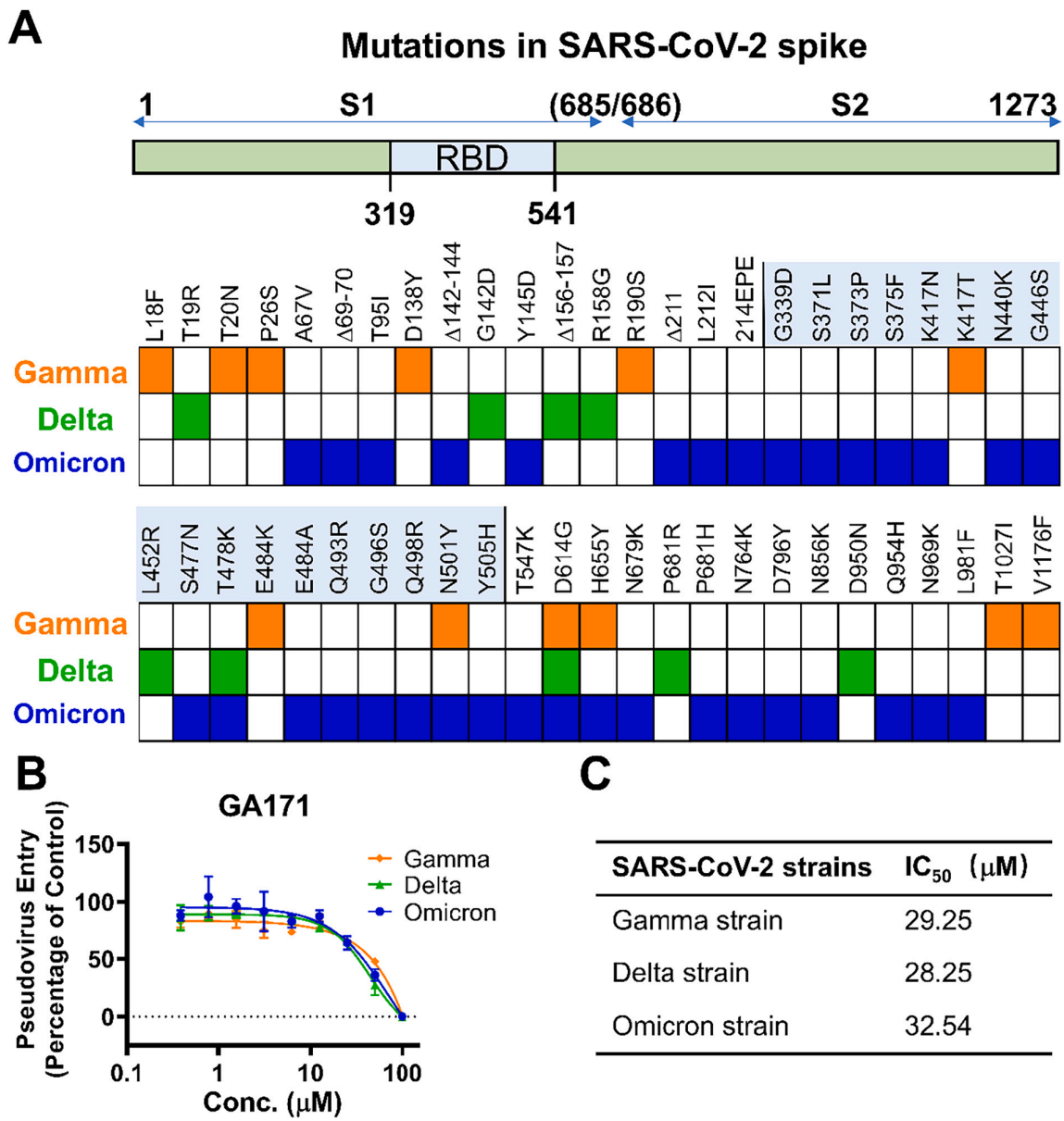

SARS-CoV-2 strains	IC_{50} (μM)
Gamma strain	29.25
Delta strain	28.25
Omicron strain	32.54

Fig. 7. Antiviral activity of GA171 against pseudo-typed Delta, Omicron, and Gamma SARS-CoV-2. (A) Comparison of residue changes of S protein in Gamma (orange), Delta (green), and Omicron (blue) variants. (B) GA171 blocked infections of hACE2/HEK293T cells by different pseudo-typed coronaviruses. (C) The IC_{50} values of GA171 in inhibiting pseudo-typed coronaviruses.

inhibition manner, implying that they are mixed-type inhibitors against SARS-CoV-2 $3CL^{pro}$ [62]. In addition, GA151 and GA150 were reported to be dual inhibitors against SARS-CoV-2 $3CL^{pro}$ and PL^{pro}, showing the ability to inhibit the replication of SARS-CoV-2 in vitro [19]. More importantly, GA151 acts as an irreversible inhibitor of PL^{pro} and $3CL^{pro}$, indicating that it is a covalent inhibitor [19]. Moreover, Ginkgolic acid exhibited antiviral activity against acyclovir-resistant herpes simplex virus type 1 through virucidal activity and fusion inhibition and significantly reduced the mortality of infected BABL/cJ mice [17]. Notably, Ginkgolic acid disrupts the early stage of the Alphavirus replication cycle and inhibits the expression of viral proteins structural E1 and non-structural nsP1, showing antiviral activity against the arboviruses [16]. In addition, it has been suggested that Ginkgolic acids effectively inhibit the release of inflammatory mediators and pro-inflammatory cytokines in ox-LDL-induced HUVECs, HMEC-1, and hPBMCs cells by blocking the activation of the NF-κB pathway [14,63].

Because Ginkgolic acids could inhibit SARS-CoV-2 by targeting multiple enzymes and proteins, we tried the same "blind" docking procedure on other four proteins, i.e., SARS-CoV-2 RdRp, $3CL^{pro}$, PL^{pro}, and human ACE2. However, the best docking scores of GA171 with proteins ranged from −5.0 to −6.4, and thus cannot tell which proteins the compound prefers to bind to and which is the actual binding site for a specific protein (Fig. S6). Therefore, we conducted biological experiments to evaluate the effects of GA171 on the above four proteins. As shown in Fig. S7, GA171 exhibited dose-dependent inhibition of SARS-CoV $3CL^{pro}$ and PL^{pro} with IC_{50} values of 3.80 and 17.85 μM, respectively. This suggests that GA171 exerts antiviral effects by dual targeting S-RBD/ACE2 interaction and key enzymes of viral replication. Importantly, GA171 has no effect on the catalytic activity of human ACE2, indicating the specificity and safety of GA171 for blocking S-RBD/ACE2

interaction. However, during optimizing GA171 against S-RBD, protein binding and cell inhibition of its derivatives should be further monitored for other potential targets. That would indicate whether multiple targeting helps the efficacy.

We reported for the first time that GA171 has antiviral activity against pseudo-typed SARS-CoV-2 and variants with different mutations in S protein by interfering with SARS-CoV-2 S-RBD and ACE2 interaction, implying that GA171 is a good starting point for developing small-molecule drugs against COVID-19. In addition, the potential binding sites of GA171 to S-RBD were identified by combining molecular simulations and binding experiments. GA171 lost a 25-fold binding affinity with the R403A mutated S-RBD, confirming the hot spot for the GA171 and S-RBD recognition (Fig. 5D). R403 is also crucial for S-RBD to recognize the host ACE2 by a salt bridge with ACE2's E37. The salt-bridge interaction was essential to stabilize the ACE2/S-RBD protein-protein interface, which was suggested by computational alanine scanning and structural analysis [64]. Meanwhile, our SPR experiment results showed that single-mutation Y505A abolished the binding of ACE2 (Fig. 6E), which is consistent with the results of Xu et al., who highlighted the role of residue Y505 as a decisive factor in the specific recognition of S-RBD by ACE2 [58]. Structure-based interaction energy evaluation will help us understand the interaction between S-RBD and ACE2, providing insights into the design of neutralizing antibodies or structure-based vaccine design [64]. Watanabe et al. analyzed the interactions between 12 antibodies/peptides and SARS-CoV-2 S-RBD by the fragment molecular orbital method [65]. They found that the residue Y505 on the S-RBD can interact with the residues on the antibody BD-629 Fab through XH/π interactions, providing helpful information for the design of effective neutralizing antibodies [65].

Interestingly, both sites R403 and Y505 are located in binding site 1 proposed by our simulations (Fig. 4C). Residue Y505 on S-RBD is located at the binding interface of ACE2/S-RBD and participates in forming protein-protein hydrogen bonds [64]. More importantly, Y505 and R403 directly interact with GA171, thus providing the atomic mechanism of how GA171 blocks the ACE2/S-RBD interaction. Recently, several groups also used in silico methods to locate multiple potential small-molecule inhibitors on the S-RBD surface that directly interacts with ACE2 [35,36,66]. Further optimization on GA171 may use all these chemical features to generate more potent inhibitors and improve their efficacy against SARS-CoV-2.

On this basis, pseudo-typed Delta, Omicron, and Gamma SARS-CoV-2 were constructed to evaluate the antiviral activity of GA171 against SARS-CoV-2 VOCs. The results showed that GA171 treatment entirely abolished the infectivity of Delta, Omicron, and Gamma pseudoviruses with similar IC_{50} values at 28.25, 32.54, and 29.25 μM, respectively. However, the toxicity of Ginkgolic acid limits the clinical use of *Ginkgo biloba* [67]. Liu et al. found that Ginkgolic acid is cytotoxic to HepG2 cells and primary rat hepatocytes, and cytochrome P450-mediated reactions enable GA151 metabolism to produce more cytotoxic compounds [68]. Furthermore, Berg et al. investigated the cytotoxicity and mutagenicity of GA, GA151, and GA171 [69]. The results showed that none of the three compounds had the mutagenic issue in vitro but caused cytotoxicity in V79 cells, with GA171 having the lowest toxicity (IC_{50} = 94 μM) [69]. Nonetheless, our results showed that GA171 did not exhibit apparent cytotoxicity in the normal cells, such as BEAS-2B (CC_{50} > 100 μM) and MASMCs (CC_{50} > 100 μM), which are representative of human and mouse lower airway cells (Fig. S5). In addition, Vero-E6 (CC_{50} > 200 μM) cells were also used to assess the cytotoxicity of GA171 as it is a standard cell line used in live SARS-CoV-2 infection experiments (Fig. S5). Our results highlighted again the importance of blocking the S-RBD/ACE2 interaction, and would facilitate future research on the treatment of COVID-19.

5. Conclusions

GA171 is a good starting point for further development to inhibit SARS-CoV-2 and its variants, including Delta, Gamma, and Omicron. We have revealed the antiviral mechanism of GA171 and developed atomic models for continuous optimization. Our results provide a new platform to develop new protein-protein inhibitors by targeting the pocket near R403 and Y505 of S-RBD. Further optimization of GA171 could improve its potency and enhance its antiviral activity, leading to more effective chemical entities against many epidemic variants.

CRediT authorship contribution statement

Lili Chen, Hongzhuan Chen, Jianrong Xu conceived and designed the experiments. Yusen Xiang, Guanglei Zhai, Mengge Wang, Xixiang Chen, Ruyu Wang, and Hang Xie carried out the experiments and data analysis. Yaozong Li and Amedeo Caflisch designed and carried out all the molecular simulations. Yusen Xiang, Guanglei Zhai, and Yaozong Li wrote the manuscript. Lili Chen, Jianrong Xu, Qian Zhang, Hongzhuan Chen, Guangbo Ge, Weidong Zhang, Yechun Xu and Amedeo Caflisch critically revised the manuscript.

Declaration of competing interest

The authors declare no competing interests.

Data availability

Data will be made available on request.

Acknowledgments

This work was supported by National Natural Science Foundation of China (82141203), Shanghai Municipal Science and Technology Major Project (ZD2021CY001, China), Shanghai Municipal Health Commission (ZY(2021-2023)-0103, China), the International Postdoc Grant funded by the Swedish Research Council (Grant VR 2019-00608 to Y.L., Sweden), and an Excellence grant of the Swiss National Science Foundation (310030B_189363 to A.C., Switzerland). We thank the Swedish National Infrastructure for Computing (SNIC) at the High-Performance Computing Center North (HPC2N) for providing the computational resources. We thank Dr. Huaqiang Xu for providing the SARS-CoV-2 RdRp protein.

Appendix A. Supplementary data

Supplementary data to this article can be found online at https://doi.org/10.1016/j.ijbiomac.2022.12.057.

References

[1] L. The, Facing up to long COVID, Lancet 396 (10266) (2020) 1861.
[2] A.R. Fehr, S. Perlman, Coronaviruses: an overview of their replication and pathogenesis, in: H.J. Maier, E. Bickerton, P. Britton (Eds.), Coronaviruses: Methods and Protocols, Springer New York, New York, NY, 2015, pp. 1–23.
[3] Y. Xiang, M. Wang, H. Chen, L. Chen, Potential therapeutic approaches for the early entry of SARS-CoV-2 by interrupting the interaction between the spike protein on SARS-CoV-2 and angiotensin-converting enzyme 2 (ACE2), Biochem. Pharmacol. 192 (2021), 114724.
[4] R. Yan, Y. Zhang, Y. Li, L. Xia, Y. Guo, Q. Zhou, Structural basis for the recognition of SARS-CoV-2 by full-length human ACE2, Science 367 (6485) (2020) 1444–1448.
[5] D. Wrapp, N. Wang, S. Corbett Kizzmekia, A. Goldsmith Jory, C.-L. Hsieh, O. Abiona, S. Graham Barney, S. McLellan Jason, Cryo-EM structure of the 2019-nCoV spike in the prefusion conformation, Science 367 (6483) (2020) 1260–1263.
[6] P. Zhou, X.-L. Yang, X.-G. Wang, B. Hu, L. Zhang, W. Zhang, H.-R. Si, Y. Zhu, B. Li, C.-L. Huang, H.-D. Chen, J. Chen, Y. Luo, H. Guo, R.-D. Jiang, M.-Q. Liu, Y. Chen, X.-R. Shen, X. Wang, X.-S. Zheng, K. Zhao, Q.-J. Chen, F. Deng, L.-L. Liu, B. Yan, F.-X. Zhan, Y.-Y. Wang, G.-F. Xiao, Z.-L. Shi, A pneumonia outbreak associated with a new coronavirus of probable bat origin, Nature 579 (7798) (2020) 270–273.
[7] A.C. Walls, Y.J. Park, M.A. Tortorici, A. Wall, A.T. McGuire, D. Veesler, Structure, function, and antigenicity of the SARS-CoV-2 spike glycoprotein, Cell 181 (2) (2020) 281–292.e6.
[8] S. Yu, Y. Chen, Y. Xiang, H. Lin, M. Wang, W. Ye, P. Zhang, H. Chen, G. Lin, Y. Zhu, L. Chen, J. Zhang, Pseudoephedrine and its derivatives antagonize wild and

mutated severe acute respiratory syndrome-CoV-2 viruses through blocking virus invasion and antiinflammatory effect, Phytother. Res. 35 (10) (2021) 5847–5860.
[9] C. Yang, X. Pan, X. Xu, C. Cheng, Y. Huang, L. Li, S. Jiang, W. Xu, G. Xiao, S. Liu, Salvianolic acid C potently inhibits SARS-CoV-2 infection by blocking the formation of six-helix bundle core of spike protein, Signal Transduct.Target.Ther. 5 (1) (2020) 220.
[10] W. Wang, S.-S. Li, X.-F. Xu, C. Yang, X.-G. Niu, S.-X. Yin, X.-Y. Pan, W. Xu, G.-D. Hu, C. Wang, S.-W. Liu, Danshensu alleviates pseudo-typed SARS-CoV-2 induced mouse acute lung inflammation, Acta Pharmacol. Sin. 43 (4) (2022) 771–780.
[11] S. Yu, Y. Zhu, J. Xu, G. Yao, P. Zhang, M. Wang, Y. Zhao, G. Lin, H. Chen, L. Chen, J. Zhang, Glycyrrhizic acid exerts inhibitory activity against the spike protein of SARS-CoV-2, Phytomedicine 85 (2021), 153364.
[12] M. Lyu, G. Fan, G. Xiao, T. Wang, D. Xu, J. Gao, S. Ge, Q. Li, Y. Ma, H. Zhang, J. Wang, Y. Cui, J. Zhang, Y. Zhu, B. Zhang, Traditional Chinese medicine in COVID-19, Acta Pharm. Sin. B 11 (11) (2021) 3337–3363.
[13] J.-R. Liang, H. Yang, Ginkgolic acid (GA) suppresses gastric cancer growth by inducing apoptosis and suppressing STAT3/JAK2 signaling regulated by ROS, Biomed. Pharmacother. 125 (2020), 109585.
[14] J. Li, A. Li, M. Li, Y. Liu, W. Zhao, D. Gao, Ginkgolic acid exerts an anti-inflammatory effect in human umbilical vein endothelial cells induced by ox-LDL, Pharmazie 73 (7) (2018) 408–412.
[15] J.-H. Lee, Y.-G. Kim, S.Y. Ryu, M.H. Cho, J. Lee, Ginkgolic acids and Ginkgo biloba extract inhibit Escherichia coli O157:H7 and Staphylococcus aureus biofilm formation, Int. J. Food Microbiol. 174 (2014) 47–55.
[16] D. Campos, S. Navarro, Y.Y. Llamas-González, M. Sugasti, J. González-Santamaría, Broad antiviral activity of ginkgolic acid against Chikungunya, Mayaro, Una, and Zika viruses, Viruses 12 (4) (2020) 449.
[17] M.S. Bhutta, O. Shechter, E.S. Gallo, S.D. Martin, E. Jones, G.F. Doncel, R. Borenstein, Ginkgolic acid inhibits herpes simplex virus type 1 skin infection and prevents zosteriform spread in mice, Viruses 13 (1) (2021) 86.
[18] M.S. Bhutta, D.G. Sausen, E.S. Gallo, H. Dahari, G.F. Doncel, R. Borenstein, Ginkgolic acid inhibits coronavirus strain 229E infection of human epithelial lung cells, Pharmaceuticals 14 (10) (2021) 980.
[19] Z. Chen, Q. Cui, L. Cooper, P. Zhang, H. Lee, Z. Chen, Y. Wang, X. Liu, L. Rong, R. Du, Ginkgolic acid and anacardic acid are specific covalent inhibitors of SARS-CoV-2 cysteine proteases, Cell Biosci. 11 (1) (2021) 45.
[20] J.-M. Lü, S. Yan, S. Jamaluddin, S.M. Weakley, Z. Liang, E.B. Siwak, Q. Yao, C. Chen, Ginkgolic acid inhibits HIV protease activity and HIV infection in vitro, Med. Sci. Monit. 18 (8) (2012) BR293–BR298.
[21] R. Borenstein, B.A. Hanson, R.M. Markosyan, E.S. Gallo, S.D. Narasipura, M. Bhutta, O. Shechter, N.S. Lurain, F.S. Cohen, L. Al-Harthi, D.A. Nicholson, Ginkgolic acid inhibits fusion of enveloped viruses, Sci. Rep. 10 (1) (2020) 4746.
[22] Y. Wang, M. Liu, J. Gao, Enhanced receptor binding of SARS-CoV-2 through networks of hydrogen-bonding and hydrophobic interactions, Proc. Natl. Acad. Sci. 117 (25) (2020) 13967–13974.
[23] J. Lan, X. He, Y. Ren, Z. Wang, H. Zhou, S. Fan, C. Zhu, D. Liu, B. Shao, T.-Y. Liu, Q. Wang, L. Zhang, J. Ge, T. Wang, X. Wang, Structural insights into the SARS-CoV-2 omicron RBD-ACE2 interaction, Cell Res. 32 (6) (2022) 593–595.
[24] B. Jawad, P. Adhikari, R. Podgornik, W.-Y. Ching, Binding interactions between receptor-binding domain of spike protein and human angiotensin converting enzyme-2 in omicron variant, J.Phys.Chem.Lett. 13 (17) (2022) 3915–3921.
[25] L. Wu, L. Zhou, M. Mo, T. Liu, C. Wu, C. Gong, K. Lu, L. Gong, W. Zhu, Z. Xu, SARS-CoV-2 omicron RBD shows weaker binding affinity than the currently dominant Delta variant to human ACE2, Signal Transduct.Target.Ther. 7 (1) (2022) 8.
[26] R. Singh, V.K. Bhardwaj, J. Sharma, R. Purohit, S. Kumar, In-silico evaluation of bioactive compounds from tea as potential SARS-CoV-2 nonstructural protein 16 inhibitors, J. Tradit. Complement. Med. 12 (1) (2022) 35–43.
[27] J. Sharma, V. Kumar Bhardwaj, R. Singh, V. Rajendran, R. Purohit, S. Kumar, An in-silico evaluation of different bioactive molecules of tea for their inhibition potency against non structural protein-15 of SARS-CoV-2, Food Chem. 346 (2021), 128933.
[28] R. Singh, V.K. Bhardwaj, P. Das, R. Purohit, A computational approach for rational discovery of inhibitors for non-structural protein 1 of SARS-CoV-2, Comput. Biol. Med. 135 (2021), 104555.
[29] V.K. Bhardwaj, R. Singh, J. Sharma, V. Rajendran, R. Purohit, S. Kumar, Identification of bioactive molecules from tea plant as SARS-CoV-2 main protease inhibitors, J. Biomol. Struct. Dyn. 39 (10) (2021) 3449–3458.
[30] V.K. Bhardwaj, R. Singh, P. Das, R. Purohit, Evaluation of acridinedione analogs as potential SARS-CoV-2 main protease inhibitors and their comparison with repurposed anti-viral drugs, Comput. Biol. Med. 128 (2021), 104117.
[31] R. Singh, V.K. Bhardwaj, P. Das, D. Bhattacherjee, G.V. Zyryanov, R. Purohit, Benchmarking the ability of novel compounds to inhibit SARS-CoV-2 main protease using steered molecular dynamics simulations, Comput. Biol. Med. 146 (2022), 105572.
[32] M. Chauhan, V.K. Bhardwaj, A. Kumar, V. Kumar, P. Kumar, M.G. Enayathullah, J. Thomas, J. George, B.K. Kumar, R. Purohit, A. Kumar, S. Kumar, Theaflavin 3-gallate inhibits the main protease (Mpro) of SARS-CoV-2 and reduces its count in vitro, Sci. Rep. 12 (1) (2022) 13146.
[33] R. Singh, V.K. Bhardwaj, R. Purohit, Potential of turmeric-derived compounds against RNA-dependent RNA polymerase of SARS-CoV-2: an in-silico approach, Comput. Biol. Med. 139 (2021), 104965.
[34] V.K. Bhardwaj, R. Singh, J. Sharma, V. Rajendran, R. Purohit, S. Kumar, Bioactive molecules of tea as potential inhibitors for RNA-dependent RNA polymerase of SARS-CoV-2, Front.Med. 8 (2021), 684020.
[35] R. Singh, V.K. Bhardwaj, J. Sharma, D. Kumar, R. Purohit, Identification of potential plant bioactive as SARS-CoV-2 spike protein and human ACE2 fusion inhibitors, Comput. Biol. Med. 136 (2021), 104631.
[36] S.E. Guimond, C.J. Mycroft-West, N.S. Gandhi, J.A. Tree, T.T. Le, C.M. Spalluto, M. V. Humbert, K.R. Buttigieg, N. Coombes, M.J. Elmore, M. Wand, K. Nyström, J. Said, Y.X. Setoh, A.A. Amarilla, N. Modhiran, J.D.J. Sng, M. Chhabra, P. R. Young, D.J. Rawle, M.A. Lima, E.A. Yates, R. Karlsson, R.L. Miller, Y.-H. Chen, I. Bagdonaite, Z. Yang, J. Stewart, D. Nguyen, S. Laidlaw, E. Hammond, K. Dredge, T.M.A. Wilkinson, D. Watterson, A.A. Khromykh, A. Suhrbier, M.W. Carroll, E. Trybala, T. Bergström, V. Ferro, M.A. Skidmore, J.E. Turnbull, Synthetic heparan sulfate mimetic pixatimod (PG545) potently inhibits SARS-CoV-2 by disrupting the spike–ACE2 interaction, ACS Cent.Sci. 8 (5) (2022) 527–545.
[37] J. Xiong, Y. Xiang, Z. Huang, X. Liu, M. Wang, G. Ge, H. Chen, J. Xu, M. Zheng, L. Chen, Structure-based virtual screening and identification of potential inhibitors of SARS-CoV-2 S-RBD and ACE2 interaction, Front. Chem. 9 (2021), 740702.
[38] J. Lan, J. Ge, J. Yu, S. Shan, H. Zhou, S. Fan, Q. Zhang, X. Shi, Q. Wang, L. Zhang, X. Wang, Structure of the SARS-CoV-2 spike receptor-binding domain bound to the ACE2 receptor, Nature 581 (7807) (2020) 215–220.
[39] Maestro, Schrödinger, LLC, New York, NY, 2020.
[40] M.H.M. Olsson, C.R. Søndergaard, M. Rostkowski, J.H. Jensen, PROPKA3: consistent treatment of internal and surface residues in empirical pKa predictions, J. Chem. Theory Comput. 7 (2) (2011) 525–537.
[41] ChemAxon, MarvinSketch 21.20.0. http://www.chemaxon.com, 2013. (Accessed 8 September 2022).
[42] D.R. Koes, M.P. Baumgartner, C.J. Camacho, Lessons learned in empirical scoring with smina from the CSAR 2011 benchmarking exercise, J. Chem. Inf. Model. 53 (8) (2013) 1893–1904.
[43] O. Trott, A.J. Olson, AutoDock Vina: improving the speed and accuracy of docking with a new scoring function, efficient optimization, and multithreading, J. Comput. Chem. 31 (2) (2010) 455–461.
[44] W.L. Jorgensen, J. Chandrasekhar, J.D. Madura, R.W. Impey, M.L. Klein, Comparison of simple potential functions for simulating liquid water, J. Chem. Phys. 79 (2) (1983) 926–935.
[45] K. Vanommeslaeghe, E. Hatcher, C. Acharya, S. Kundu, S. Zhong, J. Shim, E. Darian, O. Guvench, P. Lopes, I. Vorobyov, A.D. MacKerell, CHARMM general force field: a force field for drug-like molecules compatible with the CHARMM all-atom additive biological force fields, J. Comput. Chem. 31 (4) (2010) 671–690.
[46] J. Huang, A.D. MacKerell Jr., CHARMM36 all-atom additive protein force field: validation based on comparison to NMR data, J. Comput. Chem. 34 (25) (2013) 2135–2145.
[47] B.R. Brooks, C.L. Brooks, A.D. Mackerell, L. Nilsson, R.J. Petrella, B. Roux, Y. Won, G. Archontis, C. Bartels, S. Boresch, A. Caflisch, L. Caves, Q. Cui, A.R. Dinner, M. Feig, S. Fischer, J. Gao, M. Hodoscek, W. Im, K. Kuczera, T. Lazaridis, J. Ma, V. Ovchinnikov, E. Paci, R.W. Pastor, C.B. Post, J.Z. Pu, M. Schaefer, B. Tidor, R. M. Venable, H.L. Woodcock, X. Wu, W. Yang, D.M. York, M. Karplus, CHARMM: the biomolecular simulation program, J. Comput. Chem. 30 (10) (2009) 1545–1614.
[48] G.J. Martyna, D.J. Tobias, M.L. Klein, Constant-pressure molecular-dynamics algorithms, J. Chem. Phys. 101 (5) (1994) 4177–4189.
[49] S.E. Feller, Y.H. Zhang, R.W. Pastor, B.R. Brooks, Constant-pressure molecular-dynamics simulation - the Langevin Piston method, J. Chem. Phys. 103 (11) (1995) 4613–4621.
[50] W.G. Hoover, Canonical dynamics: equilibrium phase-space distributions, Phys. Rev. A 31 (3) (1985) 1695–1697.
[51] J.-P. Ryckaert, G. Ciccotti, H.J.C. Berendsen, Numerical integration of the cartesian equations of motion of a system with constraints: molecular dynamics of n-alkanes, J. Comput. Phys. 23 (3) (1977) 327–341.
[52] U. Essmann, L. Perera, M.L. Berkowitz, T. Darden, H. Lee, L.G. Pedersen, A smooth particle Mesh ewald method, J. Chem. Phys. 103 (19) (1995) 8577–8593.
[53] S. Jeon, M. Ko, J. Lee, I. Choi, Y. Byun Soo, S. Park, D. Shum, S. Kim, Identification of antiviral drug candidates against SARS-CoV-2 from FDA-approved drugs, Antimicrob. Agents Chemother. 64 (7) (2020) e00819–e00820.
[54] L. Braga, H. Ali, I. Secco, E. Chiavacci, G. Neves, D. Goldhill, R. Penn, J. M. Jimenez-Guardeño, A.M. Ortega-Prieto, R. Bussani, A. Cannatà, G. Rizzari, C. Collesi, E. Schneider, D. Arosio, A.M. Shah, W.S. Barclay, M.H. Malim, J. Burrone, M. Giacca, Drugs that inhibit TMEM16 proteins block SARS-CoV-2 spike-induced syncytia, Nature 594 (7861) (2021) 88–93.
[55] C. Hetényi, D. van der Spoel, Blind docking of drug-sized compounds to proteins with up to a thousand residues, FEBS Lett. 580 (5) (2006) 1447–1450.
[56] H. Guterres, W. Im, Improving protein-ligand docking results with high-throughput molecular dynamics simulations, J. Chem. Inf. Model. 60 (4) (2020) 2189–2198.
[57] The PyMOL Molecular Graphics System Version 2.2, Schrödinger, LLC, New York, NY, 2018.
[58] C. Xu, Y. Wang, C. Liu, C. Zhang, W. Han, X. Hong, Y. Wang, Q. Hong, S. Wang, Q. Zhao, Y. Wang, Y. Yang, K. Chen, W. Zheng, L. Kong, F. Wang, Q. Zuo, Z. Huang, Y. Cong, Conformational dynamics of SARS-CoV-2 trimeric spike glycoprotein in complex with receptor ACE2 revealed by cryo-EM, Sci. Adv. 7 (1) (2021), eabe5575.
[59] Y. Cao, J. Wang, F. Jian, T. Xiao, W. Song, A. Yisimayi, W. Huang, Q. Li, P. Wang, R. An, J. Wang, Y. Wang, X. Niu, S. Yang, H. Liang, H. Sun, T. Li, Y. Yu, Q. Cui, S. Liu, X. Yang, S. Du, Z. Zhang, X. Hao, F. Shao, R. Jin, X. Wang, J. Xiao, Y. Wang, X.S. Xie, Omicron escapes the majority of existing SARS-CoV-2 neutralizing antibodies, Nature 602 (7898) (2022) 657–663.
[60] T.N. Starr, A.J. Greaney, S.K. Hilton, D. Ellis, K.H.D. Crawford, A.S. Dingens, M. J. Navarro, J.E. Bowen, M.A. Tortorici, A.C. Walls, N.P. King, D. Veesler, J. D. Bloom, Deep mutational scanning of SARS-CoV-2 receptor binding domain

reveals constraints on folding and ACE2 binding, Cell 182 (5) (2020) 1295–1310.e20.
[61] S. Zhang, S. Qiao, J. Yu, J. Zeng, S. Shan, L. Tian, J. Lan, L. Zhang, X. Wang, Bat and pangolin coronavirus spike glycoprotein structures provide insights into SARS-CoV-2 evolution, Nat. Commun. 12 (1) (2021) 1607.
[62] Y. Xiong, G.-H. Zhu, H.-N. Wang, Q. Hu, L.-L. Chen, X.-Q. Guan, H.-L. Li, H.-Z. Chen, H. Tang, G.-B. Ge, Discovery of naturally occurring inhibitors against SARS-CoV-2 3CLpro from Ginkgo biloba leaves via large-scale screening, Fitoterapia 152 (2021), 104909.
[63] J. Zhang, J. Yan, Protective effect of ginkgolic acid in attenuating LDL induced inflammation human peripheral blood mononuclear cells via altering the NF-κB signaling pathway, Front. Pharmacol. 10 (2019) 01241.
[64] E. Laurini, D. Marson, S. Aulic, M. Fermeglia, S. Pricl, Computational alanine scanning and structural analysis of the SARS-CoV-2 spike protein/angiotensin-converting enzyme 2 complex, ACS Nano 14 (9) (2020) 11821–11830.
[65] K. Watanabe, C. Watanabe, T. Honma, Y.-S. Tian, Y. Kawashima, N. Kawashita, T. Takagi, K. Fukuzawa, Intermolecular interaction analyses on SARS-CoV-2 spike protein receptor binding domain and human angiotensin-converting enzyme 2 receptor-blocking antibody/peptide using fragment molecular orbital calculation, J.Phys.Chem.Lett. 12 (16) (2021) 4059–4066.
[66] V. Eskandari, Repurposing the natural compounds as potential therapeutic agents for COVID-19 based on the molecular docking study of the main protease and the receptor-binding domain of spike protein, J. Mol. Model. 28 (6) (2022) 153.
[67] Y. Hu, Q. Hua, G. Sun, K. Shi, H. Zhang, K. Zhao, S. Jia, Y. Dai, Q. Wu, The catalytic activity for ginkgolic acid biodegradation, homology modeling and molecular dynamic simulation of salicylic acid decarboxylase, Comput. Biol. Chem. 75 (2018) 82–90.
[68] Z.H. Liu, S. Zeng, Cytotoxicity of ginkgolic acid in HepG2 cells and primary rat hepatocytes, Toxicol. Lett. 187 (3) (2009) 131–136.
[69] K. Berg, C. Braun, I. Krug, D. Schrenk, Evaluation of the cytotoxic and mutagenic potential of three ginkgolic acids, Toxicology 327 (2015) 47–52.